JGR Atmospheres

RESEARCH ARTICLE
10.1029/2023JD040096

Exploring the Formation of High Levels of Hydroxyl Dicarboxylic Acids at an Urban Background Site in South China

Yunxi Huo[1], Xiaopu Lyu[2], Dawen Yao[3], Beining Zhou[1], Qi Yuan[1], Shun-cheng Lee[1], and Hai Guo[1]

[1]Department of Civil and Environmental Engineering, The Hong Kong Polytechnic University, Hong Kong, China, [2]Department of Geography, Hong Kong Baptist University, Hong Kong, China, [3]School of Intelligent Systems Engineering, Sun Yat-Sen University, Shenzhen, China

Key Points:

- The concentrations of hydroxyl dicarboxylic acids (OHDCA) in Hong Kong's air were among the highest in the world
- Aqueous and photochemical processes dominated OHDCA formation in the coastal and short-range continental air, respectively
- Aromatic compounds were likely one of the precursors of OHDCA in continental outflows

Supporting Information:

Supporting Information may be found in the online version of this article.

Correspondence to:

H. Guo and X. Lyu,
hai.guo@polyu.edu.hk;
xiaopu_lyu@hkbu.edu.hk

Citation:

Huo, Y., Lyu, X., Yao, D., Zhou, B., Yuan, Q., Lee, S.-c., & Guo, H. (2024). Exploring the formation of high levels of hydroxyl dicarboxylic acids at an urban background site in South China. *Journal of Geophysical Research: Atmospheres*, *129*, e2023JD040096. https://doi.org/10.1029/2023JD040096

Received 28 SEP 2023
Accepted 8 MAR 2024

Abstract Hydroxyl dicarboxylic acids (OHDCA) are ubiquitous in the atmosphere as an important constituent of secondary organic aerosol, yet the formation mechanisms remain unclear. At an urban background site on the coast of South China, we observed notable levels of OHDCA, with the highest concentration of malic acid (a typical OHDCA species) reaching 533 ng m^{-3}. In the coastal air, the correlation between OHDCA and sulfate was better ($R^2 = 0.48$) in the period when the relative humidity was higher and the sulfate size distribution was in a droplet mode, fitting the features of aqueous formation. In the short-range continental air, a significant rise in OHDCA levels from morning through early afternoon (588 ng m^{-3}) was observed under marked daytime increment of ozone that was corrected for titration loss (O_3_corr, sum of ozone and nitrogen dioxide). In addition, good correlation between OHDCA and O_3_corr was identified in this period, illuminating the role for gas-phase photochemistry in regulating OHDCA formation. Therefore, the elevated OHDCA was likely attributed to aqueous photooxidation, and the dominant factors varied under different atmospheric conditions. The precursors of OHDCA could be derived from biogenic emissions, as indicated by the correlations of OHDCA with 2-methylglyceric acid (bihourly data) and isoprene and monoterpenes (daily average data). However, anthropogenic aromatics might also be involved in OHDCA formation, especially in the short-range continental air. The formation mechanisms probed through observational evidence will be an important reference for rectifying simulations of OHDCA and its impact on air quality and climate.

Plain Language Summary Organic aerosol, a vital component of fine particulate matter, is suspended in the atmosphere. It is of widespread concern due to health and climate effects. In a coastal area generally considered clean, we observed remarkably high levels of climate-relevant hydroxyl dicarboxylic acids in organic aerosol. Different factors dominated the aqueous photochemical formation of hydroxyl dicarboxylic acids between air masses arriving at the measurement site. This provides a scientific basis for mitigating organic aerosol and its climate effects.

1. Introduction

Small molecule hydroxyl dicarboxylic acids (OHDCA), such as malic acid and tartaric acid, have been observed in many parts of the world with a wide range of concentrations, for example, 0.7 ng m^{-3} at a rural site in Northeast China to 201 ng m^{-3} at a suburban site in Hong Kong, South China for malic acid (Hu et al., 2008; Wu et al., 2020). Due to the high proportion of polar functional groups, that is, hydroxyl (OH) and carboxyl, in the molecules, OHDCA is expected to be more soluble than oxalic acid (the most studied analog of OHDCA) and may play critical roles in affecting the physical and chemical properties of ambient aerosols. It has been indicated that the viscosity of organic aerosol (OA) particles increases with the addition of OH group, which may further alter ice nucleation pathways and radiation intensity of cirrus layers (Reid et al., 2018; Rothfuss & Petters, 2017). Like the presence of oxalic acid in cloud condensation nuclei, OHDCA may also affect weather and climate through its involvement in cloud formation (Novakov & Penner, 1993; O'Dowd et al., 2004; Ramanathan et al., 2001). However, modeling studies generally underestimate the abundance of dicarboxylic acids in the atmosphere (Ervens et al., 2004, 2011; Zhu et al., 2020). Such modeling flaws may be the result of improper representation of their formation and degradation chemistry (Carlton et al., 2009; Varga et al., 2007).

OHDCA species in the atmosphere are generally considered as secondary products (Kawamura & Bikkina, 2016; Yao et al., 2004). In laboratory reaction systems, they were detected in ozonolysis of cycloalkanes and photo-oxidation of anthropogenic volatile organic compounds (VOCs), such as toluene, but the yields were fairly low, that is, 0.05%–0.1% (Gao et al., 2004; Sato et al., 2007). Malic acid, an OHDCA representative, was frequently observed in field campaigns and was proposed to be a late-generation photochemical oxidation product of unsaturated fatty acids and biogenic hydrocarbons (Kawamura & Ikushima, 1993). Besides, it was considered to be formed via aqueous reactions involving hydroxylation of dicarboxylic acids with similar structures (Kawamura, Sempere, et al., 1996). For example, succinic acid was suspected to be an earlier generation product of malic acid, due to the good consistency between them across many observations (Kawamura, Kasukabe, & Barrie, 1996; Kourtchev et al., 2009). Chamber studies indicated more efficient oxidation of succinic acid in aqueous phase than in gas phase (Carlton et al., 2007).

In Hong Kong, Hu and Yu (2013) first reported high levels of malic acid and speculated its formation through aqueous photodegradation of biogenic hydrocarbons, based on the correlations with secondary OA (SOA) tracers in daily samples. However, the aqueous processes were not substantiated by observational evidence. Moreover, other mechanisms that may also be involved in malic acid formation, for example, photochemical oxidation, were not discussed. Recently, we measured more OHDCA species at a higher time resolution (i.e., 1.5 hr) with a Thermal desorption Aerosol Gas chromatograph-Time of Flight-Mass Spectrometer (TAG) in the urban background atmosphere of Hong Kong. The preliminary study demonstrated that OHDCA formation was related to the levels of titration-corrected ozone (O_3_corr), which was calculated as the sum of ozone (O_3) and nitrogen dioxide (NO_2), and could be facilitated by sulfur dioxide (SO_2) in marine air (Lyu et al., 2020). While these studies shed light on OHDCA chemistry, the major mechanisms and precursors that lead to OHDCA formation under varying atmospheric conditions remain unresolved.

In this work, we explored the formation mechanisms of OHDCA with a focus on a few typical species at a coastal location in South China (Hok Tsui, hereinafter referred to as HT) that receives continental outflows in cold seasons. The study was based on a 2-month field campaign that deployed a set of state-of-the-art instruments to measure organic compounds spanning a wide range of volatility at high chemical and time resolutions. The comprehensive measurements allowed to explore the OHDCA chemistry, including formation mechanisms and potential precursors, in the real atmosphere.

2. Materials and Methods

2.1. Overview of the Sampling Campaign

From 27th September to 17th November 2020, a comprehensive sampling campaign with the main purpose of studying secondary air pollution was conducted at the urban background site HT. The site was located on the southeastern tip of Hong Kong Island, facing the South China Sea (Figure S1 in Supporting Information S1). The sampling period roughly corresponded to the time of year when photochemical air pollution was the most serious and the O_3 levels were the highest in Hong Kong (Gao et al., 2020). In autumn, northerly winds prevail in South China and bring continental air to the site (Wang et al., 2019). Thus, the observed air pollution was not only related to local emissions and chemistry, but also to air masses from the China mainland. A suite of online instruments was utilized to measure air pollutants in both gaseous and condensed phases simultaneously. The non-refractory compositions of submicron particulate matter (PM_1) were analyzed by a High Resolution-Time of Flight-Aerosol Mass Spectrometry (AMS), and we employed a TAG to measure speciated OA markers in fine particulate matter ($PM_{2.5}$). The TAG was manufactured by the Aerodyne Research Inc. and incorporated sample collection, online derivatization, thermal desorption, and chemical analysis in an operation cycle (Lyu et al., 2020). VOCs were determined by a Proton Transfer Reaction-Time of flight-Mass Spectrometer (PTR). Besides, carbon monoxide (CO), nitric oxide (NO), NO_2, O_3, SO_2, $PM_{2.5}$, and meteorological parameters were continuously monitored by the Hong Kong Environmental Protection Department (Table S1 in Supporting Information S1).

As a function of particulate matter (PM) compositions and meteorological conditions, aerosol liquid water content (LWC) was calculated using the Extended Aerosol Inorganics Model IV (E-AIM), accessible at http://www.aim.env.uea.ac.uk/aim/model4/model4a.php (Wexler & Clegg, 2002). The model inputs included the ionic compositions measured by the AMS (sulfate, nitrate, and chloride), temperature, and relative humidity. The model assumed particle neutrality through using ammonium to balance the excess anions and cations. The estimated and observed ammonium were in good agreement, with a slope and R^2 of 0.97 and 0.99, respectively. More details about

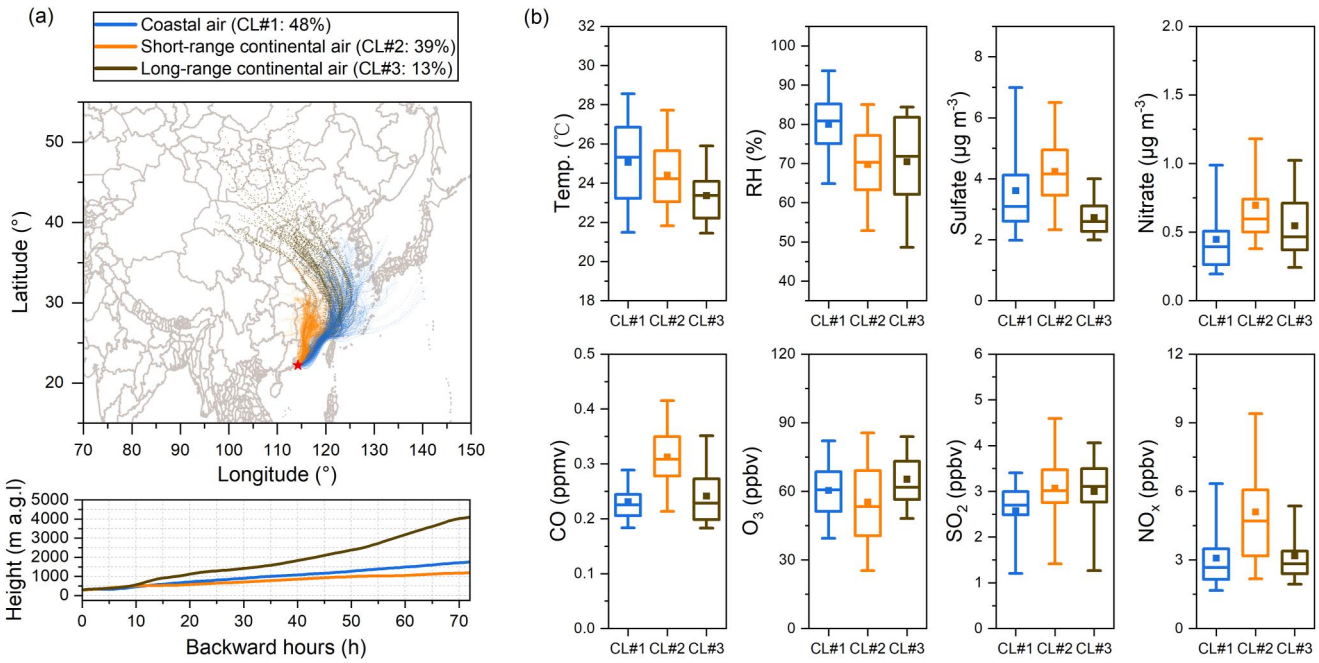

Figure 1. Distribution of the 72-hr backward trajectories arriving at HT at 300 m above ground level (a): percentages in the brackets indicate the fractions of specific types of air in total air masses by frequency; Box plot of selected meteorological parameters and air pollutants (b): square and line in the box denotes mean and median value, respectively; upper (lower) boundary of the box represents the 75th (25th) percentile; top and bottom whisker indicates the 95th and 5th percentile, respectively.

the LWC calculation can be found in Yao et al. (2022). Since the AMS data were adopted as input, the calculated LWC is bounded by PM_1 in this study. It is known that AMS cannot detect sea-salt chloride. We also calculated the LWC based on the concentrations of water-soluble ions analyzed from 28 daily filter samples of $PM_{2.5}$. Despite the difference in average values, which is expectable, the LWC derived from two sets of data correlated moderately with each other ($R^2 = 0.52$), and the LWC relationships between different types of air masses were the same.

The 72-hr backward trajectories of the air masses arriving at the site were simulated every 2 hr using a Hybrid Single-Particle Lagrangian Integrated Trajectory (HYSPLIT) model. The starting point of all the trajectories was set as 300 m above the HT site, which was in the middle and lower part of the marine boundary layer (Jury & Walker, 1988; Wang et al., 2019). Based on the model clustering, three types of air masses were identified, and we extracted all the bihourly trajectories, as shown in Figure 1. The coastal air (CL#1), short-range continental air (CL#2), and long-range continental air (CL#3) accounted for 49%, 38%, and 13% of the total air masses by frequency, respectively. While both were considered continental, the trajectories for CL#2 were largely confined to eastern and southern China, and CL#3 could be traced to northern China and even Mongolia within 72 hr. As expected, the coastal CL#1 was characterized by highest temperature (Temp.), relative humidity (RH), and LWC. CL#2 contained higher levels of anthropogenic air pollutants, for example, sulfate, nitrate, CO, SO_2, and nitrogen oxides (NO_x). Besides, CL#3 brought the coldest air from northern China to Hong Kong and contained the lowest levels of LWC and sulfate. Further, the earlier period of the CL#1 segments significantly differed from the later period with much higher levels of OHDCA and LWC, and it is marked as Stage I in contrast to Stage II for the later period. The CL#2 segments in October featured higher photolysis frequency of NO_2 (jNO_2) than that in November, which are marked as Stage III and Stage IV, respectively. The two stages also differed significantly in terms of O_3_corr. While the average O_3_corr was lower in Stage III, the daytime increment of O_3_corr from the morning to the afternoon was much larger than that in Stage IV (37.2 ppbv vs. 25.9 ppbv), implying the difference in daytime photochemical intensity. The division of stages facilitates the discussion on OHDCA formation (see Section 3.2). Table S2 in Supporting Information S1 lists the segments of different clusters and stages.

2.2. TAG Operation and Data Processing

TAG ran on a bihourly cycle, although it allowed higher time resolutions in other applications (Huo et al., 2022). The sacrifice of time resolution was to increase the sampling duration, thereby detecting more low-concentration

OA markers at this background site. Each cycle consisted of 90 min of sample collection at a flow rate of 10 L min^{-1} and 30 min of sample derivatization and transfer. The previous sample was analyzed within the first 25 min of the next sample collection, so no additional time was spent. The main steps and key parameter settings of a TAG cycle are summarized in Table S3 in Supporting Information S1, and a schematic diagram of this TAG system was provided elsewhere (Lyu et al., 2020). With integration of thermal desorption and on-line derivatization, TAG enabled in situ measurement of speciated OA molecular markers (Williams et al., 2006; Zhao et al., 2013). We adopted N-methyl-N-(trimethylsilyl)trifluoroacetamide (MSTFA) that has been widely used in other studies (e.g., Isaacman et al., 2014) as the derivatization reagent. MSTFA is suitable for thermal desorption system, due to the relatively high volatility of itself and the byproducts (Docherty & Ziemann, 2001). The fraction of helium flow with MSTFA was set as 80%–100% of the total purge flow, so that full derivatization could be achieved even for compounds containing 3–4 OH groups (Isaacman et al., 2014). As a verification, no OHDCA species was detected in its underivatized form, same for levoglucosan which could be discerned in TAG chromatograms without derivatization. Desensitization and peak drift were common problems of TAG. To track the changes, a mix of concentration-constant internal standards (IS) was injected on top of each sample or external standards (for calibration only) and analyzed simultaneously. The IS mixture was composed of 26 deuterated compounds with volatility equivalent to C_{16}–C_{36} *n*-alkanes and multiple chemical structures referenced to target compounds.

A total of 502 valid ambient samples were analyzed by TAG in the campaign. Through investigating the chromatograms, we identified 62 compounds and performed peak fitting and integration for them. They include 5 OHDCA species: citramalic acid, malic acid, 2-hydroxyglutaric acid, and two isomers of tartaric acid. Authentic or surrogate standards with 5 concentration spans, also known as external standards, were analyzed in the same way as ambient samples. The data were used to make the response—concentration curves (calibration curves). The peak areas of the target compounds and external standards were scaled by those of corresponding IS. Hence, the influence of sensitivity variation was eliminated from the temporal variations. The quantification ion, retention time, IS, R^2 of calibration curve, and average concentration for 43 quantified species are listed in Table S4 in Supporting Information S1. More information on quality control of TAG data can be found in a previous publication (Lyu et al., 2020).

The AMS and PTR applications are described in Text S1 in Supporting Information S1. Although the AMS and TAG had different cut-off sizes, the two data sets were used in combination, due to the presence of most organics in PM_1 (Cabada, et al., 2004; Timonen et al., 2008). The same treatment has also been adopted in previous studies (Huang et al., 2021; Yee et al., 2020). The AMS and PTR measurements had much higher time resolutions than TAG analysis. For matching purpose, the AMS and PTR data were averaged when necessary within each time window of TAG sample collection.

3. Results and Discussion

3.1. High Levels of Particulate OHDCA in Hong Kong

As listed in Table S4 in Supporting Information S1, the average concentration of individual OHDCA species was 197.2 ± 18.6 ng m^{-3} for a tartaric acid isomer, 186.2 ± 14.3 for another tartaric acid isomer, 84.9 ± 6.8 ng m^{-3} for malic acid, 45.6 ± 3.9 ng m^{-3} for 2-hydroxyglutaric acid, and 8.3 ± 0.7 ng m^{-3} for citramalic acid in descending order. Except for citramalic acid, the concentrations of OHDCA species were significantly higher than those of the other OA markers we detected. The total concentration of the five OHDCA species varied from 9 to 3,290 ng m^{-3} with an average (±95% Confidence Interval, CI) of 521 ± 43 ng m^{-3}. This value was even higher than the concentration of oxalic acid averaged over five Chinese megacities in summer 2018 (413 ng m^{-3}, Xu et al., 2022) and that measured at an urban site in Guangzhou, a megacity in South China and ∼120 km to the northwest of Hong Kong, in autumn 2018 (475 ng m^{-3}, J. Liu et al., 2021). These OHDCA species were also observed with high concentrations in PM_1 at the same site in a previous study (Lyu et al., 2020), and dominated over many other OA markers measured in South China (Liao & Yu, 2020; Wang, He, et al., 2017).

Figure 2 shows the time series of OHDCA species, along with the variations of PM_1 compositions, trace gases, and meteorological parameters over the sampling period. The time segments with different clusters and stages of air masses are labeled. Northeast winds dominated the whole sampling period, bringing the continental air or continental outflows along the coastline to the site, both of which were considered to be laden with various air pollutants. The average temperature and RH were 24.6°C and 75.1%, respectively. Both were noticeably higher

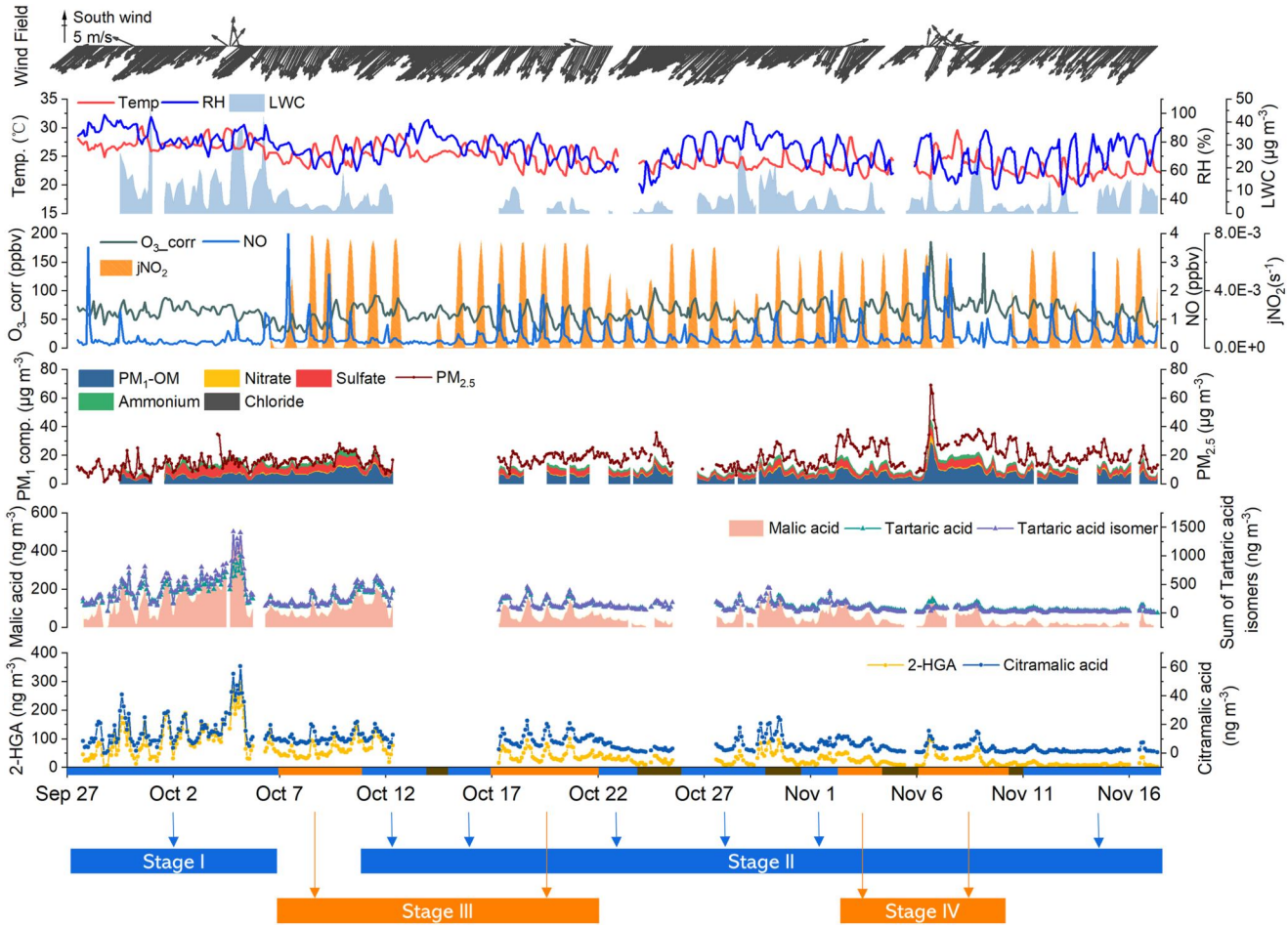

Figure 2. Time series of OHDCA species, other selected air pollutants, and meteorological parameters during the observation period. Blue, orange, and brown bar on the bottom axis represents the period with CL#1, CL#2, and CL#3 air masses, respectively. Segmentation of the CL#1 and CL#2 cases is illustrated in Section 2.1. Missing data are due to instrument maintenance.

than the national average temperature of 15.2°C and RH of 69.0% in autumn 2020 (National Bureau of Statistics of China, 2021). As expected for an autumn sampling campaign, the temperature and RH were higher in the earlier period, when higher levels of OHDCA were observed, especially before 7th Oct. This was in line with the temporal pattern of the 2018 measurements (Lyu et al., 2020). The total concentration of OHDCA correlated moderately with temperature (R^2 = 0.47), implying temperature-dependence of the formation and/or precursor emissions. The temporal variations were consistent among all the OHDCA species. In this study, the PM_1-bound organic matter (PM_1-OM) was 6.1 ± 0.3 μg m^{-3}, which was 50 ± 3% of the total concentration of the non-refractory composition. Due to the presence of other constituents, the $PM_{2.5}$, PM_1, and even PM_1-OM did not follow the variation of OHDCA. For example, in the afternoon of 6th Nov., affected by a typhoon off the east coast of Hong Kong, $PM_{2.5}$, PM_1, and PM_1-OM all increased drastically, while the increase in OHDCA was less significant. Such discrepancy indicated that the sources and chemistry of OHDCA differed from most PM components by mass. It is noteworthy that the highest levels of OHDCA were observed between the evening of 4th Oct. and the morning of 5th Oct., when a cold front approached. Meanwhile, the RH, LWC and sulfate were elevated, as expected for warm moist air before a cold front, indicating the likelihood of enhanced aqueous processes. As the cold front passed, the OHDCA concentration decreased by 50% within 2 hr due to strong winds and rainfall.

By the category of air masses, we found that the coastal air (CL#1) had the highest concentration of OHDCA (670.5 ± 86.0 ng m^{-3}), followed by the short-range continental air (CL#2, 475.8 ± 40.8 ng m^{-3}), and the long-range continental air (CL#3, 184.8 ± 30.6 ng m^{-3}). In fact, the concentrations of individual OHDCA species were

not significantly different between CL#1 and CL#2, except for the two isomers of tartaric acid (450.9 ± 55.3 ng m^{-3} in CL#1 vs. 336.3 ± 30.8 ng m^{-3} in CL#2). Tartaric acid, with the same carbon skeleton as malic acid and one more OH group, has a higher oxidation state than malic acid. To compare the chemical age of air masses, we calculated the ratio of xylenes to ethylbenzene (X/E) that signifies more aged air with lower ratio (Monod et al., 2001). It turned out to be 0.87 in CL#1 and 1.22 in CL#2. Besides, the oxygen to carbon (O/C) ratio of PM_1-OM measured by AMS was higher in CL#1 (0.81) than that in CL#2 (0.76), reiterating that the CL#1 air was more aged. Studies have demonstrated the importance of chlorine chemistry in coastal areas (Peng et al., 2022; Xue et al., 2015). However, chlorine-initiated oxidations of unsaturated aliphatic VOCs including isoprene may not lead to OHDCA formation due to the addition of chlorine atom(s) into the main products (Guo et al., 2020; Wang et al., 2022). The ratio of toluene to benzene (T/B) was calculated to examine this effect, as the reaction between benzene and chlorine is very slow (Xue et al., 2015). The difference in T/B ratio between CL#1 (1.83) and CL#2 (2.23) corroborated the different aging degrees of the two types of air masses, which however was no more significant than the difference in X/E ratio. In fact, we would expect a lower T/B ratio in CL#1, assuming that the proportional difference in T/B ratio between the CL#1 and CL#2 was consistent with that in the X/E ratio. This was still an overestimation, because the reaction rate constant of toluene with OH was ∼4.7 times that of benzene with OH, while the difference between xylenes and ethylbenzene was less than a factor of 2. Thus, the chlorine-initiated oxidation of VOCs did not appear to be more significant in CL#1 than in CL#2. This is not surprising given the presence of large sources of chlorine in the continental air that has been confirmed at this site, such as nitryl chloride photolysis and oxidation of chloride by aqueous OH radical generated from particulate nitrate photolysis (Peng et al., 2022; Xue et al., 2015). Therefore, the higher levels of OHDCA in CL#1, especially tartaric acid, were likely a result of higher degree of chemical aging that allowed OHDCA formation.

Of the OHDCA species we detected, malic acid was the most commonly studied, and its bihourly concentration reached up to 533 ng m^{-3} in this study. Here, we integrate the literature data and examine the world distribution of malic acid (Figure 3 and Table S5 in Supporting Information S1). Since both biogenic and anthropogenic VOCs could be the precursors of malic acid, the annual average emissions of isoprene, monoterpenes, and anthropogenic non-methane VOCs (NMVOCs) in 2020 (year of field measurement in this study) are also plotted to provide a background information for interpreting the malic acid distribution. However, completely matching the timing of VOC emissions and malic acid measurements is impossible, because the latter spanned decades. Thus, the VOC emissions can only be used as a rough reference. It should also be noted that the differences in sampling time, analytical methods, site categories, and particle size complicate the comparison of malic acid concentrations between studies. We try to minimize these interferences in the discussions below. For example, the high concentrations of malic acid in Hong Kong are evidenced by not only the TAG data but also the traditional gas chromatography—mass spectrometry analysis results.

Bearing the uncertainties in mind, we noticed that the concentration of malic acid varied by more than two orders of magnitude at these sites and was much higher in Asia. Moreover, eight of the top 10 concentrations were reported in China, including the highest of all 201 ng m^{-3} measured at a suburban site in Hong Kong in Jul–Aug 2006 (Hu et al., 2008). The subsequent studies have repeatedly confirmed the elevated levels of malic acid at several locations in Hong Kong (Hu & Yu, 2013; Lyu et al., 2020). High concentrations of malic acid were also observed in Shanghai and Beijing (Yu et al., 2021; Zhu et al., 2023), where the biogenic emissions were expected to be lower. In particular, the measurement in Shanghai was conducted at an urban site in a cold season (Nov–Jan), reducing the likelihood of high biogenic contributions to malic acid in that study period. In contrast, at a forest site on Changbai mountain with sparse anthropogenic emissions, the average concentration of malic acid was as high as 109 ng m^{-3} (Wang et al., 2008). Similarly, an average of 115 ng m^{-3} of malic acid was observed in a Brazilian pasture (Graham et al., 2002). Both evidences implied that biogenic emissions could also be the precursors of malic acid. However, not all the forest or mountainous sites featured elevated concentrations of malic acid, same for the sites with potentially strong anthropogenic emissions, as shown in Table S5 in Supporting Information S1. This might be because the distribution of malic acid was also regulated by other factors, such as atmospheric oxidation capacity. Ground-level measurement and modeling indicated serious O_3 pollution in eastern China (Gaudel et al., 2018; Lyu et al., 2023). Although O_3 is not necessarily a main oxidant involved in malic acid formation, it to some extent reflects the abundance of many other oxidants, for example, OH radical. Therefore, it is likely that the high levels of malic acid in several Chinese cities were partially attributable to the strong atmospheric oxidation capacity.

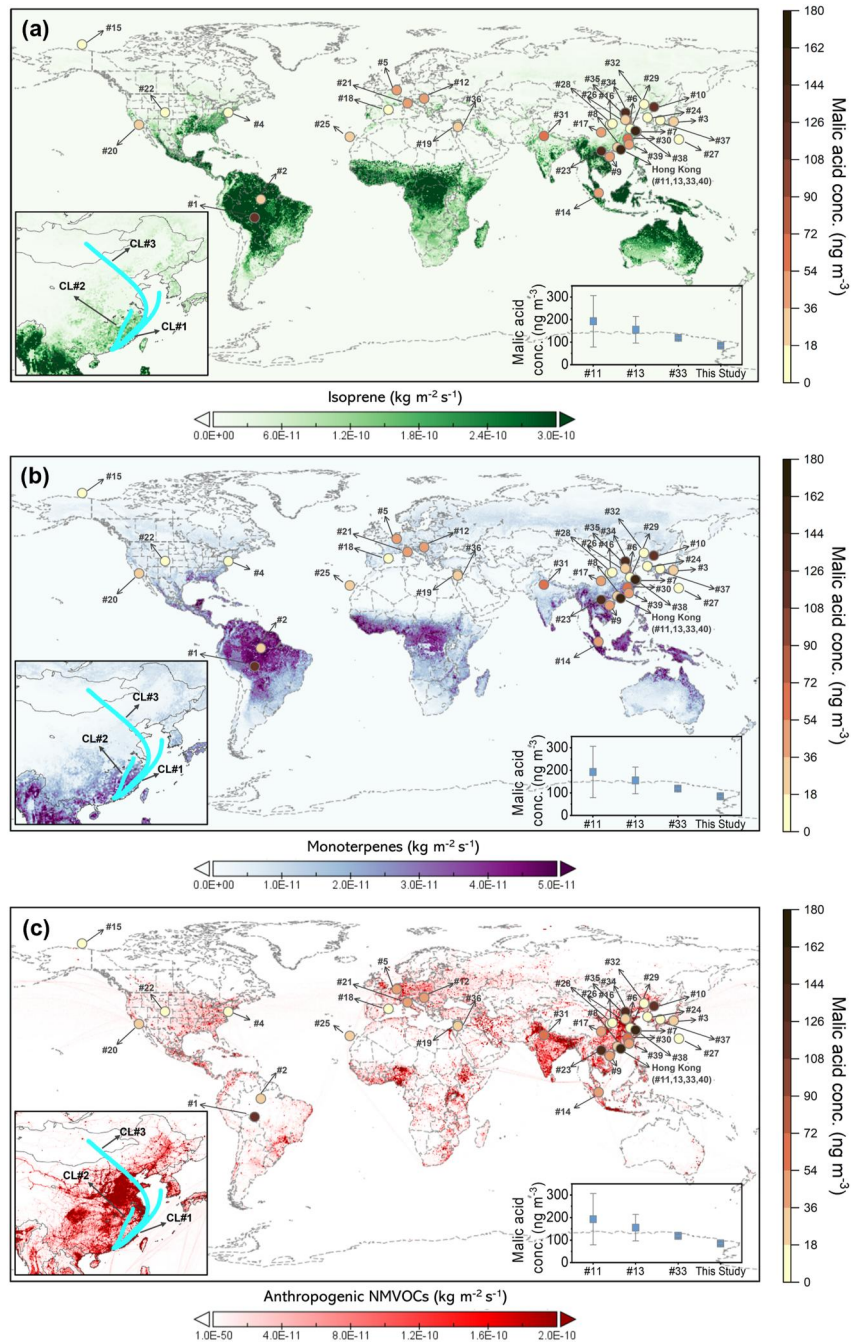

Figure 3. Global distribution of malic acid concentrations on the map of annual average emissions of isoprene (a), monoterpenes (sum of α-pinene and β-pinene) (b), and anthropogenic NMVOCs (c) in 2020 (year of field measurement in this study). The data for Hong Kong is a mean value of malic acid concentrations reported in several studies, which are shown in the inset. The VOC emission fluxes are downloaded from the Emissions of atmospheric Compounds and Compilation of Ancillary Data available at https://eccad.sedoo.fr/ (Granier et al., 2019; Sindelarova et al., 2022). Average 72-hr backward trajectories of the three clusters are shown in the lower left inset. The studies are numbered chronologically according to publication or sampling time. A detailed description of the data is summarized in Table S5 in Supporting Information S1.

Besides, biomass burning was found to increase malic acid concentration, such as that observed at a suburban site in Vietnam, that is, 128 ng m^{-3} (Nguyen et al., 2016). Nevertheless, it was rare in Hong Kong, and we did not find any relationship between malic acid and biomass burning tracers (e.g., levoglucosan) in the OHDCA-rich CL#1 and CL#2 air. Meteorological conditions play a critical role in regulating SOA formation. Water-soluble organics,

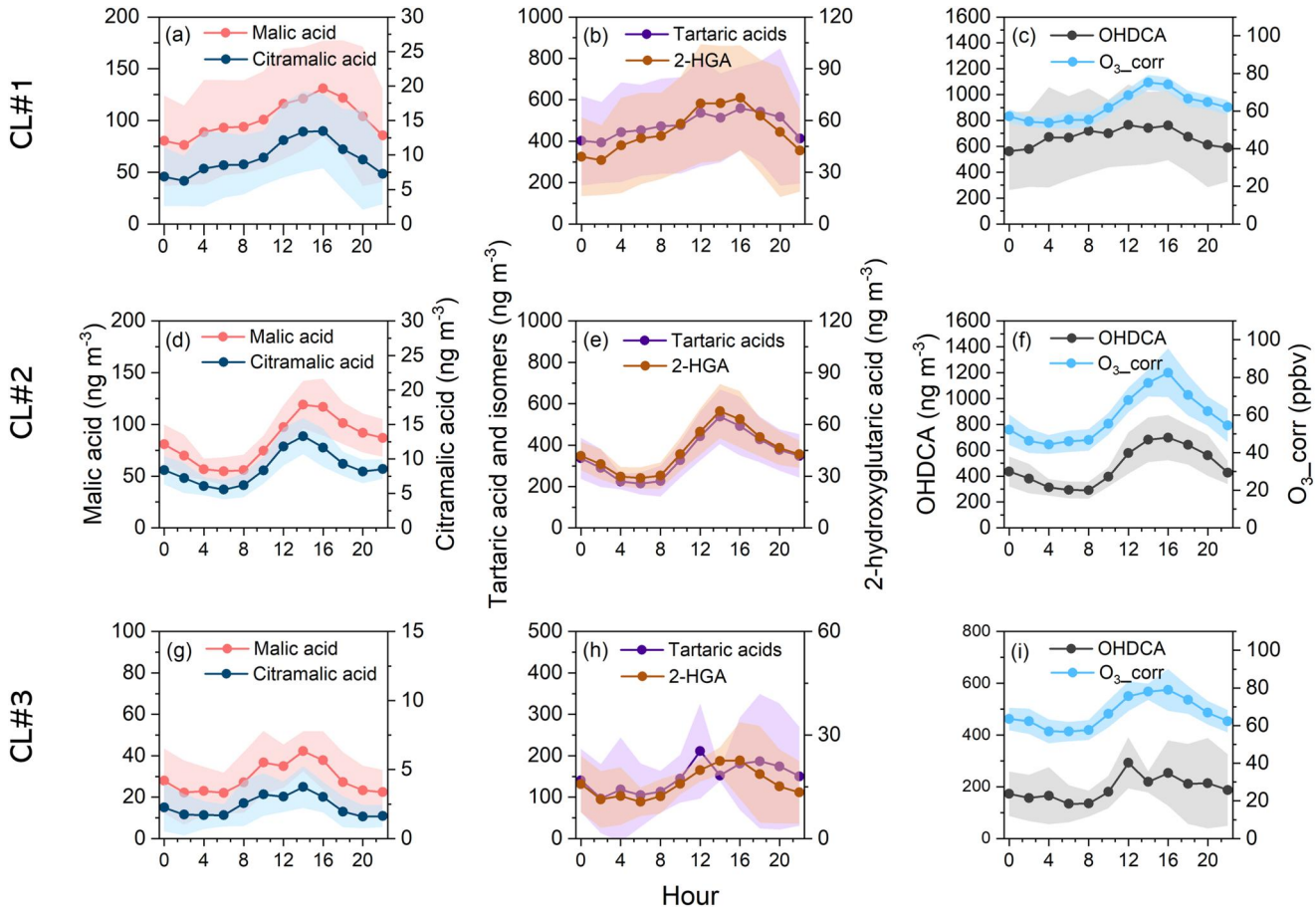

Figure 4. Diurnal variations of OHDCA species and O_3_corr in separate clusters. Shaded areas denote 95% confidence intervals.

such as oxalic acid, were found to increase under high relative humidity (Wang, Wang, et al., 2017; Xu et al., 2022). As a subtropical coastal city, Hong Kong's autumn is warm and humid, which might have also favored OHDCA formation, especially for the case of CL#1. Thus, there may be multiple factors underpinning the high levels of malic acid in Hong Kong. Moreover, the effects of all the influencing factors were blended during the transport of air masses to this background site, and the observed OHDCA might be partially attributed to emissions and chemistry in the whole region or even further afield. As an effort to unravel this mystery, we next explore the formation mechanisms of OHDCA by types of air masses.

3.2. Different Factors Dominating OHDCA Formation

The OHDCA species correlated well with each other (R^2 = 0.80–0.96) and exhibited bell-shaped diurnal patterns with afternoon peaks at 14:00–16:00, implying the secondary formation origin (Figure 4). In the coastal air (CL#1), the baseline level (lowest value in the average diurnal cycle) of OHDCA was relatively high, with the minimum to maximum ratio of 0.84. This might be due to the retention of aged air masses in the coastal area, where OHDCA could be formed through oxidation of the precursors in continental outflows.

To explore the formation mechanisms of OHDCA, we first examined the correlations between OHDCA and some secondary air pollutants, as listed in Table 1. The OHDCA species were moderately correlated with sulfate when the coastal air reached the site (R^2 = 0.53–0.67). Similar correlation was also reported for oxalic acid and considered as an evidence of in-cloud formation processes (Yu et al., 2005; Zhou et al., 2015). It has been documented that sulfate formed through aqueous reactions (e.g., in-cloud and fog processes) tends to be distributed in droplet mode (0.56–1 μm), compared to that formed from gas-phase oxidation in condensation mode (0.32–0.56 μm) (T. Liu et al., 2021; Meng & Seinfeld, 1994; Wang et al., 2016; Yu et al., 2005). In the CL#1 air masses, sulfate distribution was in a droplet mode with the mass modal diameter (d, diameter size at which the

Table 1
Summary of R^2 for the Correlations Between OHDCA Species and Selected Secondary Atmospheric Components

		Secondary inorganic ions		Oxidant	Isoprene SOA tracers			Monoterpenes SOA tracers		Anthropogenic SOA tracers	
		Sulfate	Nitrate	O_3_corr	2-MGA	2-MTs	C_5 alkenetriols	Pinic acid	MBTCA	DHOPA	Phthalic acid
CL#1	Malic acid	0.67	<0.10	0.10	0.70	0.22	0.41	0.43	0.33	0.11	<0.10
	Citramalic acid	0.53	<0.10	0.10	0.58	0.22	0.41	0.58	0.37	0.27	<0.10
	Tartaric acid	0.58	<0.10	0.10	0.64	0.19	0.39	0.40	0.30	0.10	<0.10
	2-HGA	0.65	<0.10	0.10	0.68	0.20	0.40	0.51	0.31	0.15	<0.10
CL#2	Malic acid	0.18	<0.10	0.20	0.66	<0.10	0.40	0.62	0.40	0.48	0.31
	Citramalic acid	0.11	<0.10	<0.10	0.34	<0.10	0.28	0.67	0.40	0.63	0.35
	Tartaric acid	<0.10	<0.10	<0.10	0.41	<0.10	0.27	0.51	0.35	0.31	0.12
	2-HGA	0.18	<0.10	0.12	0.54	<0.10	0.38	0.56	0.52	0.53	0.36
CL#3	Malic acid	0.37	0.39	0.44	0.13	<0.10	0.19	0.72	<0.10	0.68	0.31
	Citramalic acid	0.48	0.45	0.41	0.16	<0.10	0.24	0.68	<0.10	0.79	0.41
	Tartaric acid	0.19	0.13	0.32	<0.10	<0.10	<0.10	0.68	0.35	0.18	0.14
	2-HGA	0.34	0.34	0.53	<0.10	<0.10	<0.10	0.77	0.48	0.33	0.29

Note. 2-HGA: 2-hydroxyglutaric acid; 2-MGA: 2-methylglyceric acid; 2-MTs: 2-methyltetrols; MBTCA: 3-methyl-1,2,3-butsnetricarboxylic acid; DHOPA: 2,3-dihydroxy-4-oxopentanoic acid.

highest concentration occurs) of 0.62 μm in the earlier period (Stage I, see Section 2.1) when the RH and LWC were higher (Figure 5a and Table S6 in Supporting Information S1). The distribution shifted to a condensation mode ($d = 0.36$ μm) in the later period with CL#1 air (Stage II). As expected for aqueous formation of sulfate, the sulfur oxidation ratio (molar ratio of sulfate to the sum of sulfate and SO_2) was higher in Stage I (Figure S2 in Supporting Information S1). Most importantly, higher concentrations of OHDCA and a better correlation of OHDCA with sulfate were observed in Stage I (Figure 5b). Overall, the evidence points to aqueous formation of OHDCA in the coastal air with high LWC. Nevertheless, the OHDCA concentration was higher in daytime, opposite to the diurnal pattern of LWC (Figure S3 in Supporting Information S1). Thus, it was photochemical rather than dark (nocturnal) aqueous reactions that dominated the OHDCA formation.

In contrast, OHDCA experienced a more significant increase from morning to afternoon in CL#2, with a minimum to maximum ratio of 0.52 and net increment of 588 ng m^{-3} in the average diurnal cycle (Figure 4). The same went for O_3_corr, which increased by 35.7 ppbv (77%) between the morning trough and the afternoon peak, compared to 19.9 ppbv (36%) for CL#1 and 21.3 ppbv (37%) for CL#3. Our previous work indicated a moderate correlation ($R^2 = 0.50$) between OHDCA and O_3_corr in continental air at the same site (Lyu et al., 2020). However, in this field campaign, OHDCA did not show concordance with O_3_corr ($R^2 < 0.20$) in CL#2. This is somewhat counterintuitive, due to the synchronized diurnal patterns between them. Through investigating the day-to-day variations, we found that OHDCA correlated well with O_3_corr ($R^2 = 0.71$) in CL#2 air in the earlier period (Stage III) when the jNO_2 was the highest throughout the sampling campaign (Table S6 in Supporting Information S1), but the correlation was significantly weakened in the later period (Stage IV), as shown in Figure 5c. While the maximum O_3_corr levels were comparable in both stages, the O_3_corr increment from morning to afternoon was markedly higher in Stage III (Figure 5d), indicating more intense photochemistry. Note that the OHDCA concentration was also noticeably higher on these days. Similar consistency was also reported for oxalic acid and O_3, which was taken as evidence that gas-phase precursors or O_3-initiated oxidations mediate oxalic acid formation (Cheng et al., 2017; Yang et al., 2022). Unlike the Stage I of CL#1, OHDCA showed no correlation with sulfate in the Stage III of CL#2. The SO_2 concentration and sulfur oxidation ratio were comparable between the two periods, although the sulfate concentration in Stage III was slightly lower (Table S6 in Supporting Information S1). Moreover, we noticed a droplet-mode distribution of sulfate in Stage III (Figure S4 in Supporting Information S1). Therefore, it was plausible that sulfate in the sampled air was also formed via aqueous or in-cloud processes, while the RH and LWC were much lower (Table S6 in Supporting Information S1). The poor correlation of OHDCA with sulfate in Stage III suggested that the dominant factors in OHDCA formation were different from those in Stage I. Gas-phase precursors formed in photochemical reactions or O_3-

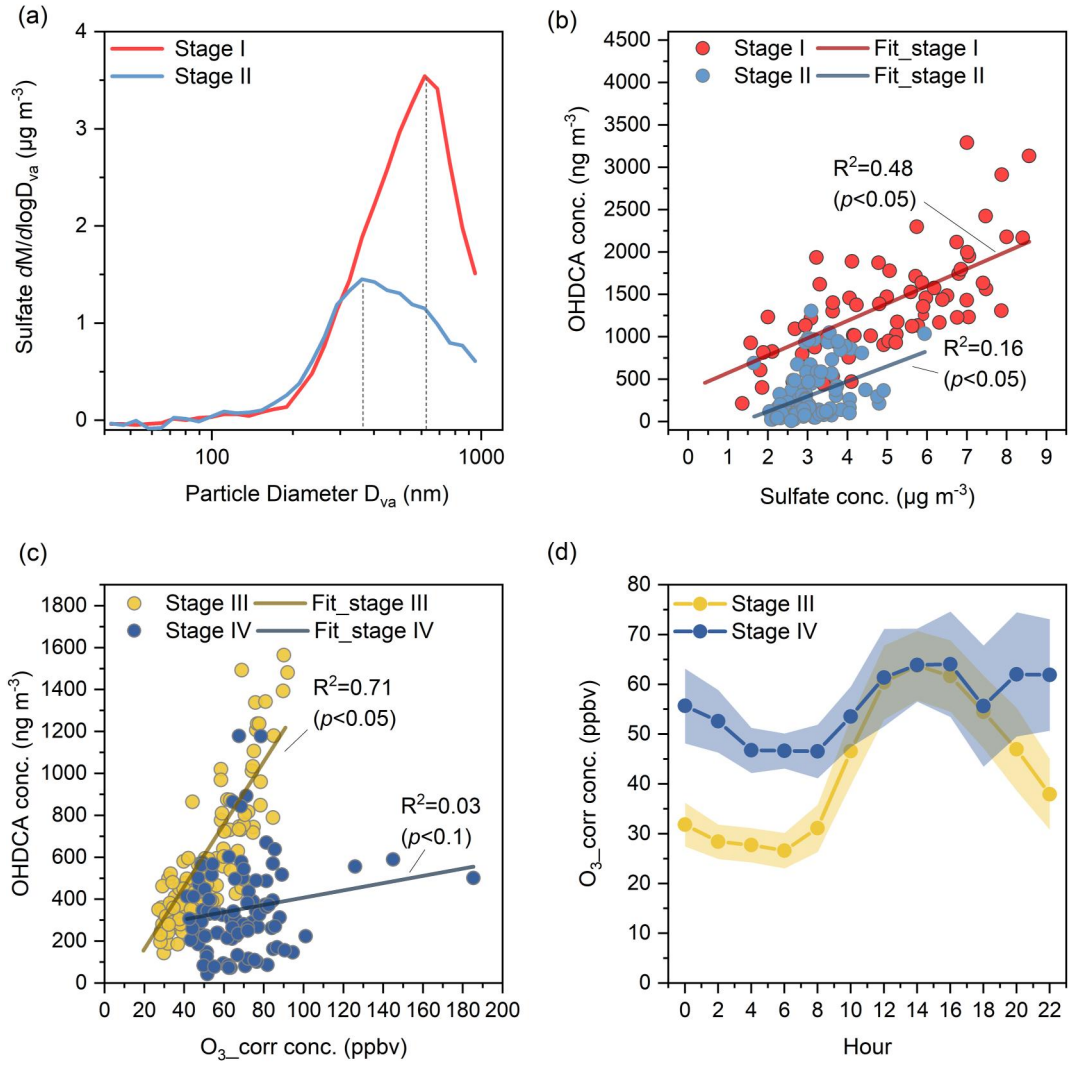

Figure 5. Size distribution of sulfate in the range of <1 μm measured by AMS (see Text S1 in Supporting Information S1) in Stage I and Stage II (a); Correlation between OHDCA and sulfate in Stage I and Stage II (b); Correlation between OHDCA and O_3_corr in Stage III and Stage IV (c); and Average diurnal cycles of O_3_corr in Stage III and Stage IV (d). Mass modal diameter of sulfate distribution is shown with the dotted line in (a).

initiated oxidations might be the primary factor regulating OHDCA formation, as indicated by the good correlation between OHDCA and O_3_corr. It is noteworthy that this conclusion does not necessarily exclude the involvement of aqueous processes in OHDCA formation in Stage III, which might occur after the precursors were partitioned into the aqueous phase.

The OHDCA concentrations in Stage II and Stage IV were relatively low (Table S6 in Supporting Information S1) and might represent background levels in the coastal air and short-range continental air, respectively. The relationships of OHDCA with O_3_corr and sulfate in the two periods appeared to reflect a mixed effect of the situations discussed above. Taken together, aqueous photooxidation was identified to be the main mechanism of OHDCA formation and was more discernible when the OHDCA concentrations were high. However, the dominant factors differed between the coastal Stage I and the continental Stage III under different atmospheric conditions. On one hand, our analysis based on observational data highlighted the importance of aqueous processes in OHDCA formation in the coastal air that were only proposed in chamber studies before (Gao et al., 2004; Sato et al., 2007). On the other hand, the effects of photochemical production of gas-phase precursors or O_3-initiated oxidations on OHDCA formation were more pronounced in the short-range continental air.

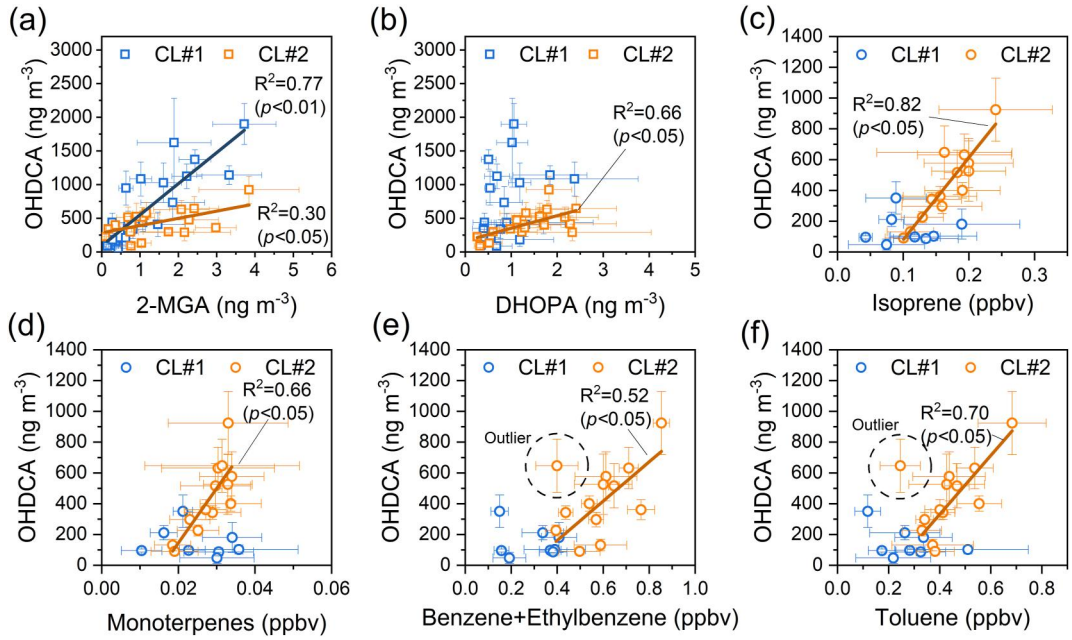

Figure 6. Scatter plot of daily average concentration of OHDCA versus SOA tracers and VOC precursors, including 2-MGA (a), DHOPA (b), isoprene (c), monoterpenes (d), benzene and ethylbenzene (e), and toluene (f). Error bars represent 95% CIs. An outlier with much higher RH that may be influenced by aqueous processes is excluded from the regression for CL#2 data points.

As mentioned above, the CL#3 air contained the lowest concentrations of OHDCA. In addition to moderate correlations with sulfate and O_3_corr, OHDCA in CL#3 also correlated with several other compounds, including not only secondary (e.g., pinic acid and DHOPA) but also primary species (e.g., CO and levoglucosan) (Figure S5 in Supporting Information S1). This phenomenon implied their common dependence on atmospheric mixing and migration. Besides, some intertwined processes could not be ruled out. For example, biomass burning might enhance the emissions of OHDCA and/or the precursors (Fu et al., 2012; Wu et al., 2020), resulting in a correlation between OHDCA and levoglucosan. Similar mechanisms were proposed to interpret the correlations between biogenic SOA species and biomass burning tracers (Ding et al., 2016).

3.3. Potential Precursors of OHDCA

An important question after the above discussion is what the precursors of OHDCA were. We attempt to answer it by examining the relationships of OHDCA with a series of chemical signatures. In both CL#1 and CL#2 air, at least moderate correlations were identified between OHDCA species and 2-MGA (Figure 6 and Table 1), a tracer of isoprene SOA formed under high-NO_x conditions (Kroll et al., 2006). Hu and Yu (2013) ever reported a better correlation between malic acid and the sum of three isoprene SOA tracers, that is, 2-MGA and two isomers of 2-MTs, based on daily data in summer ($R^2 = 0.89$). However, the formation pathways and atmospheric behaviors of 2-MGA and 2-MTs were quite different, because the latter are oxidation products of isoprene in a low-NO_x environment (Claeys et al., 2004). Consistent with the 2018 measurement results at this site (Lyu et al., 2020), higher levels of 2-MTs were observed at night, opposite to the diurnal pattern of 2-MGA. This explained the little relationship between OHDCA and 2-MTs, and the worse correlation of OHDCA with C_5 alkenetriols (Table 1), which are also isoprene SOA tracers under low NO_x conditions (Claeys et al., 2004). In addition, OHDCA had a moderate correlation with pinic acid ($R^2 = 0.39$–0.67) and a weaker correlation with MBTCA, an earlier and later generation SOA product of monoterpenes, respectively (Mutzel et al., 2016). The results suggested that biogenic VOCs might be the precursors of OHDCA, but the specific transformation pathways over multiple generations remain to be revealed.

A notable phenomenon that differentiated CL#2 from CL#1 was the better correlations between OHDCA and anthropogenic SOA tracers derived from aromatics in CL#2, that is, DHOPA and phthalic acid (Kleindienst et al., 2004, 2012). As shown in Figure S6 in Supporting Information S1, both DHOPA and phthalic acid

exhibited typical photochemical diurnal patterns. The correlation of phthalic acid with two common tracers of primary emissions, black carbon and carbon monoxide ($R^2 = 0.28$ and 0.12), was much worse than with DHOPA ($R^2 = 0.65$). Besides, terephthalic acid, an isomer of phthalic acid, is generally derived from primary emissions (Fu et al., 2010; Sheesley et al., 2010). Here, there was little consistency between the two isomers, with an R^2 of 0.03. The evidences indicated that the observed phthalic acid was more of secondary origin. Therefore, anthropogenic VOCs, especially aromatic hydrocarbons, might have also contributed to OHDCA formation in the short-range continental air.

Due to the time required for transformation of VOCs to OA compounds and its uncertainty, it was unrealistic to expect a correlation between OHDCA and VOCs at TAG's resolution. Thus, daily averages were adopted for the analysis, as shown in Figure 6 and Figure S7 in Supporting Information S1. This method also eliminates the spurious correlations caused by similar diurnal variations unrelated to chemical linkages. No significant relationship was discerned between OHDCA and VOCs in CL#1. On one hand, VOC data were only available for 8 days in coastal air, especially unavailable on days when high levels of OHDCA were observed. On the other hand, this might be due to the fact that the observed VOCs did not represent the oxidized fractions in the more aged coastal air, as indicated by the high O/C ratio and low X/E ratio (see Section 3.1). In contrast, there existed moderate to good correlations between OHDCA and biogenic VOCs (isoprene and monoterpenes) and some anthropogenic VOCs (toluene, benzene and ethylbenzene, m/p-xylene, and cyclohexane) in the less aged CL#2 air. This did not indicate the co-emissions of OHDCA and these VOCs, due to their different diurnal patterns and bad correlations at a higher resolution (e.g., bihourly). Instead, it was plausible that these species and/or other undetected fractions that followed the same patterns as these species were the precursors of OHDCA in the short-range continental air. In particular, aromatics were highly suspected.

A recent study elucidated the formation of oxalic acid (a typical dicarboxylic acid and an analog of OHDCA) at an inland site ~150 km northwest to HT using dual carbon isotope techniques (Xu et al., 2022). It indicated that oxalic acid in coastal air was mainly of biogenic origin, but more than half of it was derived from fossil sources in continental outflows. Therefore, the conclusions we drew from the chemical signatures, albeit not quantitative, are broadly in line with the carbon isotope-based analysis results for oxalic acid, the structurally simplest analog of OHDCA.

4. Conclusions

Low molecular weight dicarboxylic acids and their oxygenated analogs in atmospheric PM have significant impacts on air quality and climate, due to their high concentrations and hygroscopicity. While numerous studies have focused on oxalic acid, the current understanding of OHDCA is markedly insufficient. Our interest in OHDCA stemmed from the discovery of their high concentrations in the Hong Kong atmosphere based on both offline and in situ measurements. The mass loadings of some individual OHDCA species were in the same order of magnitude as oxalic acid, while the total concentration of OHDCA was even higher (maximum to 3,290 ng m^{-3}). Through observational evidence, this study unraveled the aqueous photochemical formation of OHDCA and the varying dominant factors between different types of air. The precursors of OHDCA were also explored by examining the relationships with chemical fingerprints. Based on the findings, the high levels of OHDCA in Hong Kong were interpretable, albeit not quantitative. First, there were plenty of anthropogenic and biogenic air pollutants in South China and the site received continental outflows from further inland with even higher anthropogenic emissions (Figure 3). Second, the aging of air pollutants led to an increase in atmospheric oxidative capacity, as indicated by high levels of O_3_corr (61.2 ppbv). Third, the subtropical climate, especially the warm and humid weather (Section 3.1), was favorable for OHDCA formation through aqueous photochemical reactions.

Overall, this study provided observational insights into the formation mechanisms of OHDCA, corroborating and complementing a handful of chamber studies with controllable variables. It also formed cross-validation with other field observational research, such as a recent radiocarbon-based study of oxalic acid in the same region. The findings of this study will help improve the representation of OHDCA chemistry in air quality and climate models and reduce modeling uncertainties. They may also apply to other places with similar emissions and meteorological characteristics. We acknowledge the lack of more direct evidence for the formation mechanisms and

quantitative evaluation of pathway/precursor contributions to OHDCA. Therefore, more research is needed to figure out OHDCA chemical kinetics under atmospherically relevant conditions and to establish the quantitative relationships between OHDCA formation and influencing factors.

Data Availability Statement

The raw data used in this study are publicly available at https://doi.org/10.6084/m9.figshare.24847806.v1 (Huo, 2023).

Acknowledgments
This study was supported by the Research Grants Council (RGC) of the Hong Kong Special Administrative Region via the NSFC/RGC Joint Research Scheme (N_PolyU530/20) and General Research Fund (HKBU 15219621). XL acknowledges the Tier 1 Research Start-up Grants provided by Hong Kong Baptist University (162912). The authors thank the Hong Kong Environmental Protection Department for providing the trace gases and meteorological data and Aerodyne Research Inc. for instrument technical support. The feedback and input from Prof. Allen H. Goldstein at University of California at Berkeley are sincerely appreciated.

References

Cabada, J. C., Rees, S., Takahama, S., Khlystov, A., Pandis, S. N., Davidson, C. I., & Robinson, A. L. (2004). Mass size distributions and size resolved chemical composition of fine particulate matter at the Pittsburgh supersite. *Atmospheric Environment*, *38*(20), 3127–3141. https://doi.org/10.1016/j.atmosenv.2004.03.004

Carlton, A. G., Turpin, B. J., Altieri, K. E., Seitzinger, S., Reff, A., Lim, H. J., & Ervens, B. (2007). Atmospheric oxalic acid and SOA production from glyoxal: Results of aqueous photooxidation experiments. *Atmospheric Environment*, *41*(35), 7588–7602. https://doi.org/10.1016/j.atmosenv.2007.05.035

Carlton, A. G., Wiedinmyer, C., & Kroll, J. H. (2009). A review of Secondary Organic Aerosol (SOA) formation from isoprene. *Atmospheric Chemistry and Physics*, *9*(14), 4987–5005. https://doi.org/10.5194/acp-9-4987-2009

Cheng, C., Li, M., Chan, C. K., Tong, H., Chen, C., Chen, D., et al. (2017). Mixing state of oxalic acid containing particles in the rural area of Pearl River Delta, China: Implications for the formation mechanism of oxalic acid. *Atmospheric Chemistry and Physics*, *17*(15), 9519–9533. https://doi.org/10.5194/acp-17-9519-2017

Claeys, M., Graham, B., Vas, G., Wang, W., Vermeylen, R., Pashynska, V., et al. (2004). Formation of secondary organic aerosols through photooxidation of isoprene. *Science*, *303*(5661), 1173–1176. https://doi.org/10.1126/science.1092805

Ding, X., He, Q. F., Shen, R. Q., Yu, Q. Q., Zhang, Y. Q., Xin, J. Y., et al. (2016). Spatial and seasonal variations of isoprene secondary organic aerosol in China: Significant impact of biomass burning during winter. *Scientific Reports*, *6*(1), 20411. https://doi.org/10.1038/srep20411

Docherty, K. S., & Ziemann, P. J. (2001). On-line, inlet-based trimethylsilyl derivatization for gas chromatography of mono-and dicarboxylic acids. *Journal of Chromatography A*, *921*(2), 265–275. https://doi.org/10.1016/s0021-9673(01)00864-0

Ervens, B., Feingold, G., Frost, G. J., & Kreidenweis, S. M. (2004). A modeling study of aqueous production of dicarboxylic acids: 1. Chemical pathways and speciated organic mass production. *Journal of Geophysical Research*, *109*(D15), D15205. https://doi.org/10.1029/2003jd004387

Ervens, B. T. B. W. R., Turpin, B. J., & Weber, R. J. (2011). Secondary organic aerosol formation in cloud droplets and aqueous particles (aqSOA): A review of laboratory, field and model studies. *Atmospheric Chemistry and Physics*, *11*(21), 11069–11102. https://doi.org/10.5194/acp-11-11069-2011

Fu, P. Q., Kawamura, K., Chen, J., Li, J., Sun, Y. L., Liu, Y., et al. (2012). Diurnal variations of organic molecular tracers and stable carbon isotopic composition in atmospheric aerosols over Mt. Tai in the North China Plain: An influence of biomass burning. *Atmospheric Chemistry and Physics*, *12*(18), 8359–8375. https://doi.org/10.5194/acp-12-8359-2012

Fu, P. Q., Kawamura, K., Pavuluri, C. M., Swaminathan, T., & Chen, J. (2010). Molecular characterization of urban organic aerosol in tropical India: Contributions of primary emissions and secondary photooxidation. *Atmospheric Chemistry and Physics*, *10*(6), 2663–2689. https://doi.org/10.5194/acp-10-2663-2010

Gao, M., Gao, J., Zhu, B., Kumar, R., Lu, X., Song, S., et al. (2020). Ozone pollution over China and India: Seasonality and sources. *Atmospheric Chemistry and Physics*, *20*(7), 4399–4414. https://doi.org/10.5194/acp-20-4399-2020

Gao, S., Keywood, M., Ng, N. L., Surratt, J., Varutbangkul, V., Bahreini, R., et al. (2004). Low-molecular-weight and oligomeric components in secondary organic aerosol from the ozonolysis of cycloalkenes and α-pinene. *The Journal of Physical Chemistry A*, *108*(46), 10147–10164. https://doi.org/10.1021/jp047466e

Gaudel, A., Cooper, O. R., Ancellet, G., Barret, B., Boynard, A., Burrows, J. P., et al. (2018). Tropospheric ozone assessment report: Present-day distribution and trends of tropospheric ozone relevant to climate and global atmospheric chemistry model evaluation. *Elem Sci Anth*, *6*, 39. https://doi.org/10.1525/elementa.291

Graham, B., Mayol-Bracero, O. L., Guyon, P., Roberts, G. C., Decesari, S., Facchini, M. C., et al. (2002). Water-soluble organic compounds in biomass burning aerosols over Amazonia 1. Characterization by NMR and GC-MS. *Journal of Geophysical Research*, *107*(D20), LBA-14. https://doi.org/10.1029/2001jd000336

Granier, C., Darras, S., van Der Gon, H. D., Jana, D., Elguindi, N., et al. (2019). The Copernicus atmosphere monitoring service global and regional emissions (April 2019 version). (Doctoral dissertation, Copernicus Atmosphere Monitoring Service).

Guo, X., Ma, F., Liu, C., Niu, J., He, N., Chen, J., & Xie, H. B. (2020). Atmospheric oxidation mechanism and kinetics of isoprene initiated by chlorine radicals: A computational study. *Science of the Total Environment*, *712*, 136330. https://doi.org/10.1016/j.scitotenv.2019.136330

Hu, D., Bian, Q., Li, T. W., Lau, A. K., & Yu, J. Z. (2008). Contributions of isoprene, monoterpenes, β-caryophyllene, and toluene to secondary organic aerosols in Hong Kong during the summer of 2006. *Journal of Geophysical Research*, *113*(D22), D22206. https://doi.org/10.1029/2008jd010437

Hu, D., & Yu, J. Z. (2013). Secondary organic aerosol tracers and malic acid in Hong Kong: Seasonal trends and origins. *Environmental Chemistry*, *10*(5), 381–394. https://doi.org/10.1071/en13104

Huang, D. D., Zhu, S., An, J., Wang, Q., Qiao, L., Zhou, M., et al. (2021). Comparative assessment of cooking emission contributions to urban organic aerosol using online molecular tracers and aerosol mass spectrometry measurements. *Environmental Science & Technology*, *55*(21), 14526–14535. https://doi.org/10.1021/acs.est.1c03280

Huo, Y. (2023). Raw data for OHDCA study at Hok Tsui_autumn 2020 [Dataset]. *Figshare*. https://doi.org/10.6084/m9.figshare.24847806.v1

Huo, Y., Guo, H., Lyu, X., & Yao, D. (2022). Emission characteristics, sources, and airborne fate of speciated organics in particulate matters in a Hong Kong residence. *Indoor Air*, *32*(3), e13017. https://doi.org/10.1111/ina.13017

Isaacman, G., Kreisberg, N. M., Yee, L. D., Worton, D. R., Chan, A. W. H., Moss, J. A., et al. (2014). Online derivatization for hourly measurements of gas-and particle-phase semi-volatile oxygenated organic compounds by thermal desorption aerosol gas chromatography (SV-TAG). *Atmospheric Measurement Techniques*, *7*(12), 4417–4429. https://doi.org/10.5194/amt-7-4417-2014

Jury, M., & Walker, N. (1988). Marine boundary layer modification across the edge of the Agulhas Current. *Journal of Geophysical Research*, *93*(C1), 647–654. https://doi.org/10.1029/jc093ic01p00647

Kawamura, K., & Bikkina, S. (2016). A review of dicarboxylic acids and related compounds in atmospheric aerosols: Molecular distributions, sources and transformation. *Atmospheric Research*, *170*, 140–160. https://doi.org/10.1016/j.atmosres.2015.11.018

Kawamura, K., & Ikushima, K. (1993). Seasonal changes in the distribution of dicarboxylic acids in the urban atmosphere. *Environmental Science & Technology*, *27*(10), 2227–2235. https://doi.org/10.1021/es00047a033

Kawamura, K., Kasukabe, H., & Barrie, L. A. (1996). Source and reaction pathways of dicarboxylic acids, ketoacids and dicarbonyls in arctic aerosols: One year of observations. *Atmospheric Environment*, *30*(10–11), 1709–1722. https://doi.org/10.1016/1352-2310(95)00395-9

Kawamura, K., Sempere, R., Imai, Y., Fujii, Y., & Hayashi, M. (1996). Water soluble dicarboxylic acids and related compounds in Antarctic aerosols. *Journal of Geophysical Research*, *101*(D13), 18721–18728. https://doi.org/10.1029/96jd01541

Kleindienst, T. E., Conver, T. S., McIver, C. D., & Edney, E. O. (2004). Determination of secondary organic aerosol products from the photooxidation of toluene and their implications in ambient $PM_{2.5}$. *Journal of Atmospheric Chemistry*, *47*(1), 79–100. https://doi.org/10.1023/b:joch.0000012305.94498.28

Kleindienst, T. E., Jaoui, M., Lewandowski, M., Offenberg, J. H., & Docherty, K. S. (2012). The formation of SOA and chemical tracer compounds from the photooxidation of naphthalene and its methyl analogs in the presence and absence of nitrogen oxides. *Atmospheric Chemistry and Physics*, *12*(18), 8711–8726. https://doi.org/10.5194/acp-12-8711-2012

Kourtchev, I., Copolovici, L., Claeys, M., & Maenhaut, W. (2009). Characterization of atmospheric aerosols at a forested site in Central Europe. *Environmental Science & Technology*, *43*(13), 4665–4671. https://doi.org/10.1021/es803055w

Kroll, J. H., Ng, N. L., Murphy, S. M., Flagan, R. C., & Seinfeld, J. H. (2006). Secondary organic aerosol formation from isoprene photooxidation. *Environmental Science & Technology*, *40*(6), 1869–1877. https://doi.org/10.1021/es0524301

Liao, K., & Yu, J. Z. (2020). Abundance and sources of benzo [a] pyrene and other PAHs in ambient air in Hong Kong: A review of 20-year measurements (1997–2016). *Chemosphere*, *259*, 127518. https://doi.org/10.1016/j.chemosphere.2020.127518

Liu, J., Zhou, S., Zhang, Z., Kawamura, K., Zhao, W., Wang, X., et al. (2021). Characterization of dicarboxylic acids, oxoacids, and α-dicarbonyls in PM2. 5 within the urban boundary layer in southern China: Sources and formation pathways. *Environmental Pollution*, *285*, 117185. https://doi.org/10.1016/j.envpol.2021.117185

Liu, T., Chan, A. W., & Abbatt, J. P. (2021). Multiphase oxidation of sulfur dioxide in aerosol particles: Implications for sulfate formation in polluted environments. *Environmental Science & Technology*, *55*(8), 4227–4242. https://doi.org/10.1021/acs.est.0c06496

Lyu, X., Guo, H., Yao, D., Lu, H., Huo, Y., Xu, W., et al. (2020). In situ measurements of molecular markers facilitate understanding of dynamic sources of atmospheric organic aerosols. *Environmental Science & Technology*, *54*(18), 11058–11069. https://doi.org/10.1021/acs.est.0c02277

Lyu, X., Li, K., Guo, H., Morawska, L., Zhou, B., Zeren, Y., et al. (2023). A synergistic ozone-climate control to address emerging ozone pollution challenges. *One Earth*, *6*(8), 964–977. https://doi.org/10.1016/j.oneear.2023.07.004

Meng, Z., & Seinfeld, J. H. (1994). On the source of the submicrometer droplet mode of urban and regional aerosols. *Aerosol Science and Technology*, *20*(3), 253–265. https://doi.org/10.1080/02786829408959681

Monod, A., Sive, B. C., Avino, P., Chen, T., Blake, D. R., & Rowland, F. S. (2001). Monoaromatic compounds in ambient air of various cities: A focus on correlations between the xylenes and ethylbenzene. *Atmospheric Environment*, *35*(1), 135–149. https://doi.org/10.1016/s1352-2310(00)00274-0

Mutzel, A., Rodigast, M., Iinuma, Y., Böge, O., & Herrmann, H. (2016). Monoterpene SOA-Contribution of first-generation oxidation products to formation and chemical composition. *Atmospheric Environment*, *130*, 136–144. https://doi.org/10.1016/j.atmosenv.2015.10.080

National Bureau of Statistics of China. (2021). National Bureau of Statistics of China. In *China statistic year book 2021*.

Nguyen, D. L., Kawamura, K., Ono, K., Ram, S. S., Engling, G., Lee, C. T., et al. (2016). Comprehensive $PM_{2.5}$ organic molecular composition and stable carbon isotope ratios at Sonla, Vietnam: Fingerprint of biomass burning components. *Aerosol and Air Quality Research*, *16*(11), 2618–2634. https://doi.org/10.4209/aaqr.2015.07.0459

Novakov, T., & Penner, J. E. (1993). Large contribution of organic aerosols to cloud-condensation-nuclei concentrations. *Nature*, *365*(6449), 823–826. https://doi.org/10.1038/365823a0

O'Dowd, C. D., Aalto, P. P., Yoon, Y. J., & Hämeri, K. (2004). The use of the pulse height analyser ultrafine condensation particle counter (PHA-UCPC) technique applied to sizing of nucleation mode particles of differing chemical composition. *Journal of Aerosol Science*, *35*(2), 205–216. https://doi.org/10.1016/j.jaerosci.2003.08.003

Peng, X., Wang, T., Wang, W., Ravishankara, A. R., George, C., Xia, M., et al. (2022). Photodissociation of particulate nitrate as a source of daytime tropospheric Cl_2. *Nature Communications*, *13*(1), 939. https://doi.org/10.1038/s41467-022-28383-9

Ramanathan, V. C. P. J., Crutzen, P. J., Kiehl, J. T., & Rosenfeld, D. (2001). Aerosols, climate, and the hydrological cycle. *Science*, *294*(5549), 2119–2124. https://doi.org/10.1126/science.1064034

Reid, J. P., Bertram, A. K., Topping, D. O., Laskin, A., Martin, S. T., Petters, M. D., et al. (2018). The viscosity of atmospherically relevant organic particles. *Nature Communications*, *9*(1), 956. https://doi.org/10.1038/s41467-018-03027-z

Rothfuss, N. E., & Petters, M. D. (2017). Influence of functional groups on the viscosity of organic aerosol. *Environmental Science & Technology*, *51*(1), 271–279. https://doi.org/10.1021/acs.est.6b04478

Sato, K., Hatakeyama, S., & Imamura, T. (2007). Secondary organic aerosol formation during the photooxidation of toluene: NO x dependence of chemical composition. *The Journal of Physical Chemistry A*, *111*(39), 9796–9808. https://doi.org/10.1021/jp071419f

Sheesley, R. J., DeMinter, J. T., Meiritz, M., Snyder, D. C., & Schauer, J. J. (2010). Temporal trends in motor vehicle and secondary organic tracers using in situ methylation thermal desorption GCMS. *Environmental Science & Technology*, *44*(24), 9398–9404. https://doi.org/10.1021/es102301t

Sindelarova, K., Markova, J., Simpson, D., Huszar, P., Karlicky, J., Darras, S., & Granier, C. (2022). High-resolution biogenic global emission inventory for the time period 2000–2019 for air quality modelling. *Earth System Science Data*, *14*(1), 251–270. https://doi.org/10.5194/essd-14-251-2022

Timonen, H., Saarikoski, S., Tolonen-Kivimäki, O., Aurela, M., Saarnio, K., Petäjä, T., et al. (2008). Size distributions, sources and source areas of water-soluble organic carbon in urban background air. *Atmospheric Chemistry and Physics*, *8*(18), 5635–5647. https://doi.org/10.5194/acp-8-5635-2008

Varga, Z., Kiss, G., & Hansson, H. C. (2007). Modelling the cloud condensation nucleus activity of organic acids on the basis of surface tension and osmolality measurements. *Atmospheric Chemistry and Physics*, *7*(17), 4601–4611. https://doi.org/10.5194/acp-7-4601-2007

Wang, D. S., Masoud, C. G., Modi, M., & Hildebrandt Ruiz, L. (2022). Isoprene-chlorine oxidation in the presence of NO_x and implications for urban atmospheric chemistry. *Environmental Science & Technology*, *56*(13), 9251–9264. https://doi.org/10.1021/acs.est.1c07048

Wang, G., Zhang, R., Gomez, M. E., Yang, L., Levy Zamora, M., Hu, M., et al. (2016). Persistent sulfate formation from London Fog to Chinese haze. *Proceedings of the National Academy of Sciences*, *113*(48), 13630–13635. https://doi.org/10.1073/pnas.1616540113

Wang, J., Wang, G., Gao, J., Wang, H., Ren, Y., Li, J., et al. (2017). Concentrations and stable carbon isotope compositions of oxalic acid and related SOA in Beijing before, during, and after the 2014 APEC. *Atmospheric Chemistry and Physics*, *17*(2), 981–992. https://doi.org/10.5194/acp-17-981-2017

Wang, Q., He, X., Huang, X. H., Griffith, S. M., Feng, Y., Zhang, T., et al. (2017). Impact of secondary organic aerosol tracers on tracer-based source apportionment of organic carbon and $PM_{2.5}$: A case study in the Pearl River Delta, China. *ACS Earth and Space Chemistry*, *1*(9), 562–571. https://doi.org/10.1021/acsearthspacechem.7b00088

Wang, T., Dai, J., Lam, K. S., Nan Poon, C., & Brasseur, G. P. (2019). Twenty-five years of lower tropospheric ozone observations in tropical East Asia: The influence of emissions and weather patterns. *Geophysical Research Letters*, *46*(20), 11463–11470. https://doi.org/10.1029/2019gl084459

Wang, W., Wu, M. H., Li, L., Zhang, T., Liu, X. D., Feng, J. L., et al. (2008). Polar organic tracers in $PM_{2.5}$ aerosols from forests in eastern China. *Atmospheric Chemistry and Physics*, *8*(24), 7507–7518. https://doi.org/10.5194/acp-8-7507-2008

Wexler, A. S., & Clegg, S. L. (2002). Atmospheric aerosol models for systems including the ions H^+, NH_4^+, Na^+, SO_4^{2-}, NO_3^-, Cl^-, Br^-, and H_2O. *Journal of Geophysical Research*, *107*(D14), ACH-14. https://doi.org/10.1029/2001jd000451

Williams, B. J., Goldstein, A. H., Kreisberg, N. M., & Hering, S. V. (2006). An in-situ instrument for speciated organic composition of atmospheric aerosols: Thermal desorption aerosol GC/MS-FID (TAG). *Aerosol Science and Technology*, *40*(8), 627–638. https://doi.org/10.1080/02786820600754631

Wu, X., Cao, F., Haque, M., Fan, M. Y., Zhang, S. C., & Zhang, Y. L. (2020). Molecular composition and source apportionment of fine organic aerosols in Northeast China. *Atmospheric Environment*, *239*, 117722. https://doi.org/10.1016/j.atmosenv.2020.117722

Xu, B., Zhang, G., Gustafsson, Ö., Kawamura, K., Li, J., Andersson, A., et al. (2022). Large contribution of fossil-derived components to aqueous secondary organic aerosols in China. *Nature Communications*, *13*(1), 5115. https://doi.org/10.1038/s41467-022-32863-3

Xue, L. K., Saunders, S. M., Wang, T., Gao, R., Wang, X. F., Zhang, Q. Z., & Wang, W. X. (2015). Development of a chlorine chemistry module for the master chemical mechanism. *Geoscientific Model Development*, *8*(10), 3151–3162. https://doi.org/10.5194/gmd-8-3151-2015

Yang, C., Zhou, S., Zhang, C., Yu, M., Cao, F., & Zhang, Y. (2022). Atmospheric chemistry of oxalate: Insight into the role of relative humidity and aerosol acidity from high-resolution observation. *Journal of Geophysical Research: Atmospheres*, *127*(4), e2021JD035364. https://doi.org/10.1029/2021jd035364

Yao, D., Guo, H., Lyu, X., Lu, H., & Huo, Y. (2022). Secondary organic aerosol formation at an urban background site on the coastline of South China: Precursors and aging processes. *Environmental Pollution*, *309*, 119778. https://doi.org/10.1016/j.envpol.2022.119778

Yao, X., Fang, M., Chan, C. K., Ho, K. F., & Lee, S. C. (2004). Characterization of dicarboxylic acids in $PM_{2.5}$ in Hong Kong. *Atmospheric Environment*, *38*(7), 963–970. https://doi.org/10.1016/j.atmosenv.2003.10.048

Yee, L. D., Isaacman-VanWertz, G., Wernis, R. A., Kreisberg, N. M., Glasius, M., Riva, M., et al. (2020). Natural and anthropogenically influenced isoprene oxidation in southeastern United States and central Amazon. *Environmental Science & Technology*, *54*(10), 5980–5991. https://doi.org/10.1021/acs.est.0c00805

Yu, J. Z., Huang, X. F., Xu, J., & Hu, M. (2005). When aerosol sulfate goes up, so does oxalate: Implication for the formation mechanisms of oxalate. *Environmental Science & Technology*, *39*(1), 128–133. https://doi.org/10.1021/es049559f

Yu, Q., Chen, J., Cheng, S., Qin, W., Zhang, Y., Sun, Y., & Ahmad, M. (2021). Seasonal variation of dicarboxylic acids in $PM_{2.5}$ in Beijing: Implications for the formation and aging processes of secondary organic aerosols. *Science of the Total Environment*, *763*, 142964. https://doi.org/10.1016/j.scitotenv.2020.142964

Zhao, Y., Kreisberg, N. M., Worton, D. R., Teng, A. P., Hering, S. V., & Goldstein, A. H. (2013). Development of an in situ thermal desorption gas chromatography instrument for quantifying atmospheric semi-volatile organic compounds. *Aerosol Science and Technology*, *47*(3), 258–266. https://doi.org/10.1080/02786826.2012.747673

Zhou, Y., Huang, X. H., Bian, Q., Griffith, S. M., Louie, P. K., & Yu, J. Z. (2015). Sources and atmospheric processes impacting oxalate at a suburban coastal site in Hong Kong: Insights inferred from 1 year hourly measurements. *Journal of Geophysical Research: Atmospheres*, *120*(18), 9772–9788. https://doi.org/10.1002/2015jd023531

Zhu, S., Zhou, M., Qiao, L., Huang, D. D., Wang, Q., Wang, S., et al. (2023). Evolution and chemical characteristics of organic aerosols during wintertime $PM_{2.5}$ episodes in Shanghai, China: Insights gained from online measurements of organic molecular markers. In *Atmospheric chemistry and physics discussions* (pp. 1–22).

Zhu, Y., Tilgner, A., Hoffmann, E. H., Herrmann, H., Kawamura, K., Yang, L., et al. (2020). Multiphase MCM-CAPRAM modeling of the formation and processing of secondary aerosol constituents observed during the Mt. Tai summer campaign in 2014. *Atmospheric Chemistry and Physics*, *20*(11), 6725–6747. https://doi.org/10.5194/acp-20-6725-2020

References From the Supporting Information

Alier, M., Osto, M. D., Lin, Y. H., Surratt, J. D., Tauler, R., Grimalt, J. O., & van Drooge, B. L. (2014). On the origin of water-soluble organic tracer compounds in fine aerosols in two cities: The case of Los Angeles and Barcelona. *Environmental Science and Pollution Research*, *21*(20), 11649–11660. https://doi.org/10.1007/s11356-013-2460-9

Agarwal, R., Shukla, K., Kumar, S., Aggarwal, S. G., & Kawamura, K. (2020). Chemical composition of waste burning organic aerosols at landfill and urban sites in Delhi. *Atmospheric Pollution Research*, *11*(3), 554–565. https://doi.org/10.1016/j.apr.2019.12.004

Alier, M., Van Drooge, B. L., Dall'Osto, M., Querol, X., Grimalt, J. O., & Tauler, R. (2013). Source apportionment of submicron organic aerosol at an urban background and a road site in Barcelona (Spain) during SAPUSS. *Atmospheric Chemistry and Physics*, *13*(20), 10353–10371. https://doi.org/10.5194/acp-13-10353-2013

Fu, P. Q., Kawamura, K., Chen, J., Charrière, B., & Sempéré, R. (2013). Organic molecular composition of marine aerosols over the Arctic Ocean in summer: Contributions of primary emission and secondary aerosol formation. *Biogeosciences*, *10*(2), 653–667. https://doi.org/10.5194/bg-10-653-2013

Fu, P., Kawamura, K., Okuzawa, K., Aggarwal, S. G., Wang, G., Kanaya, Y., & Wang, Z. (2008). Organic molecular compositions and temporal variations of summertime mountain aerosols over Mt. Tai, North China Plain. *Journal of Geophysical Research*, *113*(D19), D19107. https://doi.org/10.1029/2008jd009900

García, M. I., Van Drooge, B. L., Rodríguez, S., & Alastuey, A. (2017). Speciation of organic aerosols in the Saharan Air Layer and in the free troposphere westerlies. *Atmospheric Chemistry and Physics*, *17*(14), 8939–8958. https://doi.org/10.5194/acp-17-8939-2017

Haque, M. M., Kawamura, K., Deshmukh, D. K., Fang, C., Song, W., Mengying, B., & Zhang, Y. L. (2019). Characterization of organic aerosols from a Chinese megacity during winter: Predominance of fossil fuel combustion. *Atmospheric Chemistry and Physics*, *19*(7), 5147–5164. https://doi.org/10.5194/acp-19-5147-2019

Hong, Y., Xu, X., Liao, D., Liu, T., Ji, X., Xu, K., et al. (2022). Measurement report: Effects of anthropogenic emissions and environmental factors on the formation of biogenic secondary organic aerosol (BSOA) in a coastal city of southeastern China. *Atmospheric Chemistry and Physics*, *22*(11), 7827–7841. https://doi.org/10.5194/acp-22-7827-2022

Hong, Z., Zhang, H., Zhang, Y., Xu, L., Liu, T., Xiao, H., et al. (2019). Secondary organic aerosol of $PM_{2.5}$ in a mountainous forest area in southeastern China: Molecular compositions and tracers implication. *Science of the Total Environment*, *653*, 496–503. https://doi.org/10.1016/j.scitotenv.2018.10.370

Ikemori, F., Uranishi, K., Sato, T., Fujihara, M., Hasegawa, H., & Sugata, S. (2021). Time-resolved characterization of organic compounds in $PM_{2.5}$ collected at Oki Island, Japan, affected by transboundary pollution of biomass and non-biomass burning from Northeast China. *Science of the Total Environment*, *750*, 142183. https://doi.org/10.1016/j.scitotenv.2020.142183

Kim, H., Kim, J. Y., Jin, H. C., Lee, J. Y., & Lee, S. P. (2016). Seasonal variations in the light-absorbing properties of water-soluble and insoluble organic aerosols in Seoul, Korea. *Atmospheric Environment*, *129*, 234–242. https://doi.org/10.1016/j.atmosenv.2016.01.042

Kanellopoulos, P. G., Verouti, E., Chrysochou, E., Koukoulakis, K., & Bakeas, E. (2021). Primary and secondary organic aerosol in an urban/industrial site: Sources, health implications and the role of plastic enriched waste burning. *Journal of Environmental Sciences*, *99*, 222–238. https://doi.org/10.1016/j.jes.2020.06.012

Kourtchev, I., Warnke, J., Maenhaut, W., Hoffmann, T., & Claeys, M. (2008). Polar organic marker compounds in $PM_{2.5}$ aerosol from a mixed forest site in western Germany. *Chemosphere*, *73*(8), 1308–1314. https://doi.org/10.1016/j.chemosphere.2008.07.011

Li, L., Dai, D., Deng, S., Feng, J., Zhao, M., Wu, J., et al. (2013b). Concentration, distribution and variation of polar organic aerosol tracers in Ya'an, a middle-sized city in western China. *Atmospheric Research*, *120*, 29–42. https://doi.org/10.1016/j.atmosres.2012.07.024

Li, X., Liu, Y., Li, D., Wang, G., Bai, Y., Diao, H., et al. (2017). Molecular composition of organic aerosol over an agricultural site in North China Plain: Contribution of biogenic sources to $PM_{2.5}$. *Atmospheric Environment*, *164*, 448–457. https://doi.org/10.1016/j.atmosenv.2017.06.018

Li, M., McDow, S. R., Tollerud, D. J., & Mazurek, M. A. (2006). Seasonal abundance of organic molecular markers in urban particulate matter from Philadelphia, PA. *Atmospheric Environment*, *40*(13), 2260–2273. https://doi.org/10.1016/j.atmosenv.2005.10.025

Li, L., Wu, D., Chang, X., Tang, Y., Hua, Y., Xu, Q., et al. (2021). Polar organic aerosol tracers in two areas in Beijing-Tianjin-Hebei region: Concentration comparison before and in the sept. Third Parade and sources. *Environmental Pollution*, *270*, 116108. https://doi.org/10.1016/j.envpol.2020.116108

Li, J. J., Wang, G. H., Cao, J. J., Wang, X. M., & Zhang, R. J. (2013a). Observation of biogenic secondary organic aerosols in the atmosphere of a mountain site in central China: Temperature and relative humidity effects. *Atmospheric Chemistry and Physics*, *13*(22), 11535–11549. https://doi.org/10.5194/acp-13-11535-2013

Pietrogrande, M. C., Bacco, D., Visentin, M., Ferrari, S., & Casali, P. (2014). Polar organic marker compounds in atmospheric aerosol in the Po Valley during the Supersito campaigns - Part 2: Seasonal variations of sugars. *Atmospheric Environment*, *97*, 215–225. https://doi.org/10.1016/j.atmosenv.2014.07.056

Ren, Y. Q., Wang, G. H., Li, J. J., Wu, C., Cao, C., Li, J., et al. (2019). Evolution of aerosol chemistry in Xi'an during the spring dust storm periods: Implications for heterogeneous formation of secondary organic aerosols on the dust surface. *Chemosphere*, *215*, 413–421. https://doi.org/10.1016/j.chemosphere.2018.10.064

Waked, A., Afif, C., Brioude, J., Formenti, P., Chevaillier, S., Haddad, I. E., et al. (2013). Composition and source apportionment of organic aerosol in Beirut, Lebanon, during winter 2012. *Aerosol Science and Technology*, *47*(11), 1258–1266. https://doi.org/10.1080/02786826.2013.831975

Xie, M., Mladenov, N., Williams, M. W., Neff, J. C., Wasswa, J., & Hannigan, M. P. (2016). Water soluble organic aerosols in the Colorado Rocky Mountains, USA: Composition, sources and optical properties. *Scientific Reports*, *6*(1), 39339. https://doi.org/10.1038/srep39339

Yao, D., Lyu, X., Lu, H., Zeng, L., Liu, T., Chan, C. K., & Guo, H. (2021). Characteristics, sources and evolution processes of atmospheric organic aerosols at a roadside site in Hong Kong. *Atmospheric Environment*, *252*, 118298. https://doi.org/10.1016/j.atmosenv.2021.118298

Yang, L., Nguyen, D. M., Jia, S., Reid, J. S., & Liya, E. Y. (2013). Impacts of biomass burning smoke on the distributions and concentrations of C2-C5 dicarboxylic acids and dicarboxylates in a tropical urban environment. *Atmospheric Environment*, *78*, 211–218. https://doi.org/10.1016/j.atmosenv.2012.03.049